Preparations and Electrochemical Properties of Pyrazine-Bridged Ruthenium-Binuclear Complexes Exhibiting Molecular Hysteresis

Atsuko Tomita and Mitsuru Sano*

Graduate School of Human Informatics, Nagoya University, Nagoya 464-8601, Japan

Received December 11, 1998

Three binuclear Ru complexes *cis*-,*cis*-[$(NH_3)_4$(L)Ru-pz-Ru$(NH_3)_4$(dmso)]$(PF_6)_4$ (L = NH_3 (**4**), pyridine (**5**), benzonitrile (**6**); dmso = dimethyl sulfoxide) have been prepared, and their electrochemical behavior, exhibiting molecular hysteresis, is reported. Simulations of cyclic voltammograms and thin-layer cyclic voltammograms have provided redox potentials, isomerization rates, and interconversion rates of the complexes. The rates of the conversions between two isomeric intermediate states have been determined to be 5×10^{-6} and 4×10^{-4} s^{-1} for the complex **4**, 4×10^{-5} and 4×10^{-4} s^{-1} for the complex **5**, and 2×10^{-4} and 5×10^{-5} s^{-1} for the complex **6**. The equilibrium parameters between these states are discussed in relation to the redox potentials of the complexes.

A single molecule exhibiting bistability with hysteresis is of the utmost importance to the prospects for molecular memories[1] and in reaching an understanding of memory phenomena in nature. The properties of molecule **1** (Chart 1), which was specifically designed to exhibit the important features of a hysteresis loop on being addressed electrochemically, have been described.[2−5] In it are combined two Ru^{3+}/Ru^{2+} couples, one with the metal attached to the thioether function of the bridging ligand and the other with it attached to the sulfoxide. The former gives a reversible response in cyclic voltammetry, while the other has the property that on reduction, for example, isomerization of the O-bound state to S-bound takes place, this being reversed on oxidation.[6,7] When the value of $E_{1/2}$ for the reversible couple lies between the electrochemical signals for the two other couples, for which electron transfer is attended by linkage isomerization, two intermediate states arise: [Ru^{2+}- -Ru^{3+}OS], by $1e^-$ reduction of the fully oxidized molecule in its stable form [Ru^{3+}- -Ru^{3+}OS], and the other, [Ru^{3+}- -Ru^{2+}SO], by $1e^-$ oxidation of the fully reduced molecule in its stable form [Ru^{2+}- -Ru^{2+}SO]. The isomeric intermediate states can interconvert by intramolecular transfer coupled to linkage isomerization. The relationship of this behavior to loss of memory in molecular devices has been dealt with in earlier publications.[2,4,8]

Herein, we describe the electrochemical, kinetic, and thermodynamic properties of **4**−**6** with pyrazine as a bridging ligand in Chart 1. In **1** the communication between the metal centers is very weak, it being mediated by interaction through space or by the saturated bond system. This is demonstrated by the results of observations made on a variant of **1** where both sulfur atoms are in the thioether form: when the molecule is in the [3+,2+] mixed-valence form, the extinction coefficient of the intervalence band is only 6 M^{-1} cm^{-1}.[2] In **4**−**6**, the metal centers are linked by pyrazine. In marked contrast to the weak interaction

Chart 1

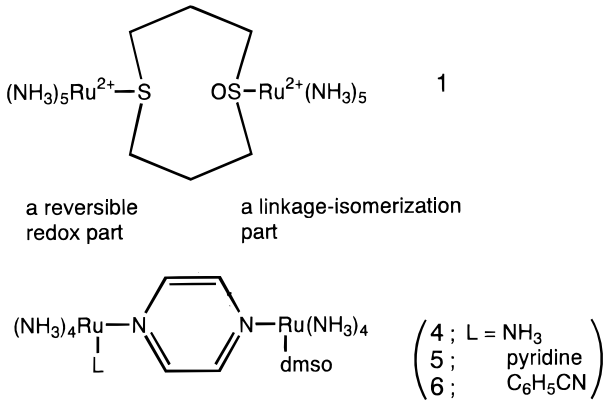

encountered for **1**, when pyrazine bridges $Ru(NH_3)_5^{3+}$ and $Ru(NH_3)_5^{2+}$ the interaction is very strong and in fact the mixed-valence molecule is considered by most to be delocalized. In **4**−**6**, the interaction will be reduced because the two redox centers are not equivalent, but it nevertheless is very much stronger that it is in **1**. Another significant change between **1** and the these compositions of present interest is that the bridging ligand, pyrazine, is a π acid, and its replacement of NH_3, a simple σ donor, at the center undergoing linkage isomerization, is expected to affect the dynamics of the system. Finally, the changes in composition of a reversible couple provide an opportunity to study the effect of driving forces on the behavior of the system, which includes an interest in the intermediate, isomeric states.

Experimental Section

Materials. [$Ru(NH_3)_5$(acetone)]$(PF_6)_2$ and *cis*-[$Ru(NH_3)_4$(methanol)$_2$]$(PF_6)_2$ were synthesized from [$Ru(NH_3)_5Cl]Cl_2$ and *cis*-[$Ru(NH_3)_4Cl_2$]Cl as described in the literature,[9,10] respectively. Pyrazine (pz) was recrystallized from ether. Dimethyl sulfoxide (dmso), pyridine (py), and benzonitrile (C_6H_5CN) were purchased from Wako Chemical and were used without further purification. Acetone was purified by vacuum distillation over B_2O_3,[11] and ethanol and methanol were purified by

(1) Kölle, U. *Angew. Chem., Int. Ed. Engl*. **1991**, *30*, 956−958.
(2) Sano, M.; Taube, H. *J. Am. Chem. Soc*. **1991**, *113*, 2327−2328.
(3) Sano, M. *Kagaku Asahi* **1991**, *51*(9), 34−37.
(4) Sano, M.; Taube, H. *Inorg. Chem.* **1994**, *33*, 705−709.
(5) Sano, M. *Polym. Adv. Technol*. **1995**, *6*, 178−184.
(6) Yeh, A.; Scott, N.; Taube, H. *Inorg. Chem*. **1982**, *21*, 2542−2545.
(7) Tomita, A.; Sano, M. Unpublished result. A single-crystal X-ray analysis has been performed for [$Ru(NH_3)_5$(*n*-butyl sulfoxide)]$(CF_3SO_3)_3$. The oxygen of the sulfoxide has been confirmed to coordinate to the Ru^{3+}.
(8) Tomita, A.; Sano, M. *Chem. Lett.* **1996**, 981−982.
(9) Callahan, R. W.; Brown, G. M.; Meyer, T. J. *Inorg. Chem*. **1975**, *14*, 1443−1453.
(10) Sugaya, T.; Sano, M. *Inorg. Chem*. **1993**, *32*, 5878−5879.

10.1021/ic9814219 CCC: $19.00
Published on Web 12/29/1999

distillation over $Mg(OCH_3)_2$ and $Mg(OC_2H_5)_2$, respectively. Anhydrous Et_2O and CH_2Cl_2 were purchased from Aldrich (Sure/Seal bottle) and were used without further purification. Tetra-1-butylammonium hexafluorophosphate (*n*-Bu_4NPF_6) (Tokyo Kasei) was recrystallized from ethanol and dried at 105 °C under vacuum. All solvents were thoroughly deoxygenated by purging with argon in a Vacuum/Atmospheres Co. inert-atmosphere dry glovebox.

All reactions and measurements were carried out under argon atmosphere in a Vacuum/Atmospheres Co. inert-atmosphere dry glovebox.

Preparation of *cis*-[Ru(NH$_3$)$_4$(dmso)(pz)](PF$_6$)$_2$ (2). *cis*-[Ru(NH$_3$)$_4$(methanol)$_2$](PF$_6$)$_2$ (90 mg) was dissolved in 0.2 mL of acetone followed by the slow addition, with stirring, of 1.5 mL of acetone solution containing 14.3 mg of dmso, and after 15 min, 5 mL of CH_2Cl_2 was added. The pale yellow precipitate (*cis*-[Ru(NH$_3$)$_4$(dmso)(acetone)](PF$_6$)$_2$, **3**) was collected by filtration and washed with CH_2Cl_2.

Compound **3** (86 mg) was dissolved in 2 mL of acetone. This was slowly added to the acetone solution (0.1 mL) containing pyrazine (71 mg) with stirring, stirring being continued for 1 h. The orange solution was treated with CH_2Cl_2 (5 mL), and the precipitate was collected by filtration and washed with CH_2Cl_2. An orange solid was obtained (76 mg).

^{1}H NMR (acetone-d_6; 25 °C): δ 8.98 (2H, d; pz), 8.59 (2H, d; pz), 3.72 (3H, br; NH_3), 3.27 (6H, s; CH_3), 3.10 (3H, br; NH_3), 2.89 (6H, br; NH_3).

Preparation of *cis*-[(NH$_3$)$_5$Ru(pz)Ru(NH$_3$)$_4$(dmso)](PF$_6$)$_4$ (4). The orange compound **2** (62.2 mg) was dissolved in 0.5 mL of acetone. An acetone solution (0.5 mL) containing [Ru(NH$_3$)$_5$(acetone)](PF$_6$)$_2$ (59.2 mg) was added, and the resulting deep red solution was stirred for 3 h in the dark. Treatment with CH_2Cl_2 (5.5 mL) resulted in a precipitate; after being collected by filtration it was dissolved in 2 mL of acetone, following which CH_2Cl_2 (2 mL) was slowly added. The solution was filtered off, and CH_2Cl_2 (3 mL) was gradually added to the filtrate. The red-purple precipitate was collected by filtration and washed with CH_2Cl_2. A red-purple solid was obtained (70 mg).

Anal. Calcd for $C_6H_{37}N_{10}SORu_2P_4F_{24}\cdot{}^1/_2(CH_3)_2CO$: C, 8.12; H, 3.64; N, 12.64. Found: C, 7.78; H, 3.57; N, 12.68. ^{1}H NMR (acetone-d_6; 25 °C): δ 8.87 (2H, d; pz), 8.29 (2H, d; pz), 3.77 (3H, br; NH_3), 3.53 (3H, br; NH_3), 3.29 (6H, s; CH_3), 3.11 (3H, br; NH_3), 2.72 (6H, br; NH_3), 2.56 (12H, br; NH_3).

Preparation of *cis*-,*cis*-[(NH$_3$)$_4$(py)Ru(pz)Ru(NH$_3$)$_4$(dmso)](PF$_6$)$_4$ (5). *cis*-[Ru(NH$_3$)$_4$(methanol)$_2$](PF$_6$)$_2$ (93.1 mg) was dissolved in 0.5 mL of acetone, and to it was added, with stirring, 3 mL of acetone containing 15 mg of pyridine. After 30 min, the solution was treated with CH_2Cl_2 (10 mL). The yellow precipitate (*cis*-[Ru(NH$_3$)$_4$(py)(acetone)](PF$_6$)$_2$) was collected by filtration and washed with CH_2Cl_2.

The above yellow compound (48.3 mg) and compound **2** (50.4 mg) were dissolved in 2 mL of acetone. The red solution was stirred for 16 h in the dark. The resulting precipitate was removed by filtration. Treatment of the filtrate with CH_2Cl_2 (10 mL) resulted in a precipitate which was collected by filtration and was redissolved in 2 mL of acetone. To the solution was slowly added CH_2Cl_2 (8 mL). The red-purple precipitate was collected by filtration and washed with CH_2Cl_2. The yield was 75 mg.

Anal. Calcd for $C_{11}H_{39}N_{11}SORu_2P_4F_{24}$: C, 11.43; H, 3.40; N, 13.34. Found: C, 11.55; H, 3.40; N, 12.62. ^{1}H NMR (acetone-d_6; 25 °C): δ 8.61 (2H, d; pz), 8.46 (2H, d; pz), 8.45 (2H, d; pz), 7.89 (1H, t; py), 7.39 (2H, t; py), 3.66 (3H, br; NH_3), 3.51 (3H, br; NH_3), 3.27 (6H, s; CH_3), 3.14 (3H, br; NH_3), 2.91 (3H, br; NH_3), 2.76 (6H, br; NH_3), 2.69 (6H, br; NH_3).

Preparation of *cis*-,*cis*-[(NH$_3$)$_4$(C$_6$H$_5$CN)Ru(pz)Ru(NH$_3$)$_4$(dmso)](PF$_6$)$_4$ (6). *cis*-[Ru(NH$_3$)$_4$(methanol)$_2$](PF$_6$)$_2$ (103 mg) was dissolved in 0.2 mL of acetone. To the solution was slowly added 2.5 mL of acetone solution containing 22.4 mg of C_6H_5CN. After 1 h, the solution was treated with CH_2Cl_2 (8 mL). The yellow precipitate (*cis*-[Ru(NH$_3$)$_4$(C$_6$H$_5$CN)(acetone)](PF$_6$)$_2$) was collected by filtration and washed with CH_2Cl_2.

The above yellow compound (106.9 mg) and compound **2** (106.2 mg) were dissolved in 3 mL of acetone, and the solution was stirred for 40 h in the dark. The red solution was treated with CH_2Cl_2 (10 mL) and ether (3 mL). The precipitate was collected by filtration and redissolved with 2 mL of acetone, and the solution was filtered. To the filtrate was gradually added CH_2Cl_2 (5 mL). The deep-red precipitation was collected by filtration and washed with CH_2Cl_2. The total yield was 146 mg.

Anal. Calcd for $C_{13}H_{39}N_{11}SORu_2P_4F_{24}$: C, 13.23; H, 3.33; N, 13.06. Found: C, 14.00; H, 3.54; N, 12.32. ^{1}H NMR (acetone-d_6; 25 °C): δ 8.94 (2H, d; pz), 8.62 (2H, d; pz), 7.85 (2H, d; C_6H_5CN), 7.70 (1H, t; C_6H_5CN), 7.57 (2H, t; C_6H_5CN), 3.54 (3H, br; NH_3), 3.45 (3H, br; NH_3), 3.27 (6H, s; CH_3), 3.18 (3H, br; NH_3), 3.10 (3H, br; NH_3), 2.80 (6H, br; NH_3), 2.74 (6H, br; NH_3).

Instrumentation. Proton NMR spectra were recorded on a JEOL α-400 spectrometer and are reported as ppm shifts from acetone-d_6 (2.04 ppm for ^{1}H). The electronic absorption spectra were recorded on a Hitachi 330 spectrophotometer.

Cyclic voltammetry and thin layer cyclic voltammetry were carried out by a BAS-100B electrochemical analyzer on acetone solutions of complexes (3 mM) containing 0.2 M *n*-Bu_4NPF_6. Cyclic voltammetries were performed by a three-electrode system with a platinum working electrode, a platinum-wire counter electrode, and a gold-wire reference electrode with the ferrocene/ferrocenium hexafluorophosphate (Fc/Fc^+) dissolved in acetone. Thin-layer cyclic voltammograms were taken on the acetone solution in an argon atmosphere. A 1 mL volume of acetone solution 1 mM in the complex and 0.5 M in *n*-Bu_4NPF_6 was admitted to the compartment of the thin (0.08 mm thickness) layer electrochemical cell equipped with a platinum 150 mesh working electrode, a counter electrode, and a reference. All potentials are reported vs the normal hydrogen electrode. The reference electrode was calibrated with the Fc/Fc^+ couple (E = 0.55 V (NHE)) as measured in situ. Variable-temperature electrochemical experiments in the drybox employed a thermostat system with an Eyela MPF-40, which controlled the temperature to $\pm$0.1 K.

All reactions and measurements were carried out under argon atmosphere in a Vacuum/Atmospheres Co. inert-atmosphere dry glovebox.

Digital Simulation for Cyclic Voltammetry. Digital simulations of proposed electrochemical mechanisms were done for cyclic voltammograms and for thin-layer cyclic voltammograms with DigiSim[12] and a general purpose program,[13] respectively. We assumed Nernstian behaviors in these simulations.

Results

Molecular Design and Preparations. The archetypal molecule exhibiting the molecular hysteresis made by our group consists of two parts, a reversible redox part and a linkage isomerization part. In our earlier work[8] the linkage isomerization function was presented by the bridging group. In the compositions chosen for the present study, this is not the case. The bridging ligand is pyrazine, where the isomerization part is Ru(NH$_3$)$_4$(dmso) and the reversible redox part is Ru(NH$_3$)$_4$L (L = NH_3, pyridine, benzonitrile). The ligand, L, changes the redox potentials, thus affecting the equilibrium constant between the mixed-valence species. We prepared the PF_6^- salts of three complexes, *cis*-,*cis*-[(NH$_3$)$_5$Ru-pz-Ru(NH$_3$)$_4$(dmso)]$^{4+}$ (**4**), *cis*-,*cis*-[(NH$_3$)$_4$(py)Ru-pz-Ru(NH$_3$)$_4$(dmso)]$^{4+}$ (**5**), and *cis*-,*cis*-[(NH$_3$)$_4$(C$_6$H$_5$CN)Ru-pz-Ru(NH$_3$)$_4$(dmso)]$^{4+}$ (**6**).

Scheme 1 summarizes the preparative strategy. The majority of preparations described in the Experimental Section utilize as a synthetic intermediate *cis*-[Ru(NH$_3$)$_4$(methanol)$_2$](PF$_6$)$_2$[14] dissolved in acetone. The reactions in acetone, *cis*-[Ru(NH$_3$)$_4$(acetone)$_2$]$^{2+}$ + L → *cis*-[Ru(NH$_3$)$_4$(L)(acetone)]$^{2+}$ + acetone,

(11) Burfield, D. R.; Smithers, R. H. *J. Org. Chem*. **1978**, *43*, 3966−3968.

(12) DigiSim from Bioanalytical Systems, Inc., is a simulation program for cyclic voltammetry.

(13) Bard, A. J.; Faulkner, L. R. *Electrochemical Methods, Fundamentals and Applications*; Wiley: New York, 1980; p 675.

(14) At room temperature, the methanol complex can be stored for 1 week as a solid under argon.

Scheme 1

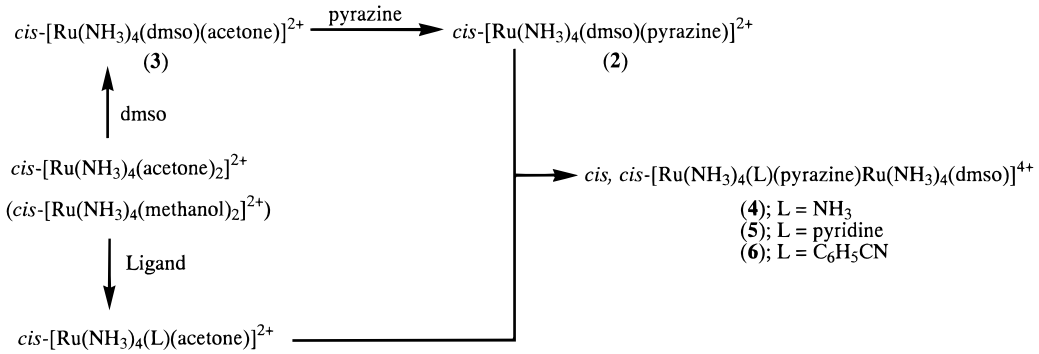

Scheme 2

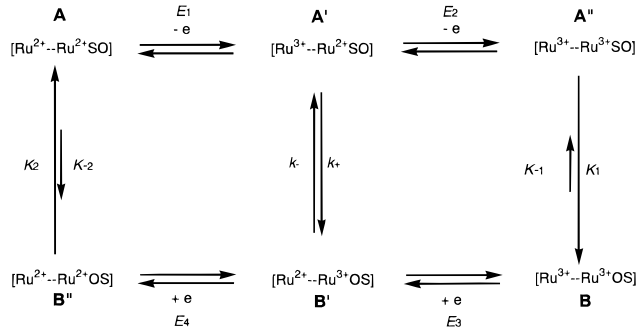

are rapid and apparently quantitative. The new strategy is particularly useful when the entering ligand is insoluble in water. Acetone is readily replaced from *cis*-$[Ru(NH_3)_4(L)(acetone)]^{2+}$ to form derivatives of the type *cis*-$[Ru(NH_3)_4(L)(L')]^{2+}$. The desired binuclear compounds are prepared by the reaction with *cis*-$[Ru(NH_3)_4(dmso)(pyrazine)]^{2+}$ and *cis*-$[Ru(NH_3)_4(acetone)(L)]^{2+}$.

Electrochemical Behavior of the Complex 5. Two examples of cyclic voltammetry traces are presented in Figure 1a,c for 3 mM acetone solutions of the fully reduced form ($[Ru^{2+}\text{-}\,\text{-}Ru^{2+}\text{-}SO]$) and the fully oxidized form ($[Ru^{3+}\text{-}\,\text{-}Ru^{3+}OS]$) of the complex **5**. This electrochemical behavior is understandable according to Scheme 2. At a scan rate of 100 mV s^{-1}, the electrochemical behavior of the fully oxidized form (Figure 1c) is simpler and will be dealt with first. Starting at oxidizing potentials, two reversible couples are observed, one at $E_{1/2} = 0.92$ V, peak to peak separation 0.10 V, which is assigned to $[Ru^{3+/2+}\text{-}\,\text{-}Ru^{3+}OS]$, and the other at $E_{1/2} = 0.45$ V, $\Delta V = 0.09$ V, assigned to $[Ru^{2+}\text{-}\,\text{-}Ru^{3+/2+}OS]$. The fact that no complications are observed shows that isomerization of $Ru^{2+}OS$ to Ru^{2+}-SO is slow on the time scale defined by the sweep rate. In starting with the fully reduced form, E_a at 0.87 V is assigned to $[Ru^{2+}\text{-}\,\text{-}Ru^{2+}SO] \rightarrow [Ru^{3+}\text{-}\,\text{-}Ru^{2+}SO]$, close to, but not identical with, the corresponding value of $E_a = 0.97$ V in Figure 1c. The oxidation $[Ru^{3+}\text{-}\,\text{-}Ru^{2+}SO] \rightarrow [Ru^{3+}\text{-}\,\text{-}Ru^{3+}SO]$ takes place at $E_a = 1.55$ V with no corresponding reduction wave on reversing the sweep, owing to rapid isomerization of $Ru^{3+}SO$ to $Ru^{3+}OS$. On the reverse scan, only a small signal of $E_c = 0.87$ V for the process $[Ru^{3+}\text{-}\,\text{-}Ru^{3+}OS] \rightarrow [Ru^{2+}\text{-}\,\text{-}Ru^{3+}OS]$ is observed, owing to loss by diffusion from the electrode, and a larger signal of $E_c = 0.79$ V ascribable to $[Ru^{3+}\text{-}\,\text{-}Ru^{2+}SO] \rightarrow [Ru^{2+}\text{-}\,\text{-}Ru^{2+}SO]$. A wave at about 0.45 V is assigned to $[Ru^{2+}\text{-}\,\text{-}Ru^{3+/2+}OS]$; it is weak because of loss by diffusion from the electrode.

To extract values of the dynamic parameters, the cyclic voltammograms for the fully reduced and the fully oxidized forms were digitally simulated according to Scheme 2. In these simulations, experimental redox potentials were used, and rates of the isomerizations and of heterogeneous electron transfers on electrode are parametrized, while the interconversions between **A′** and **B′** were neglected. Figure 1b,d shows two examples of the fitting results. Experimental and simulated results give fair agreement showing that the proposed scheme is reasonable and the interconversions are so slow as to be negligible. The linkage isomerization rates were also estimated in these fitting processes.[16] The CV result for the other compounds were digitally simulated in the above manner, and the rates of the isomerizations were also obtained as given in Tables 1 and 2.

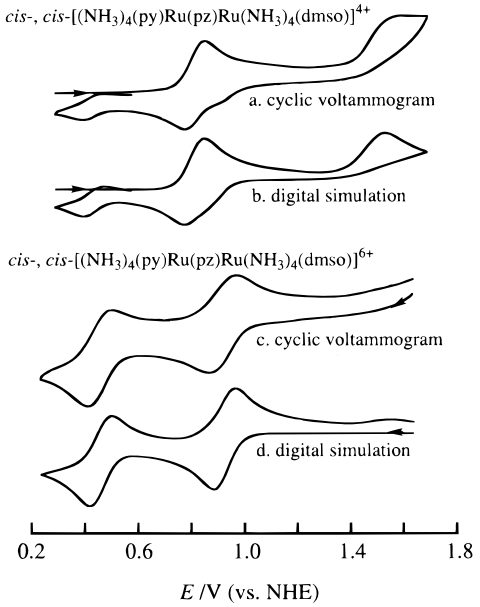

Figure 1. Cyclic voltammograms and digital simulations at 100 mV s^{-1} on acetone solutions containing *cis*-,*cis*-$[(NH_3)_4(py)Ru(pz)Ru(NH_3)_4(dmso)]^{4+/6+}$ (3 mM) and *n*-Bu_4NPF_6 (0.2 M) at 25 °C.

Rates of Conversions between the Mixed-Valence Species. It is important to know the rates of the interconversion of **A′** and **B′** in Scheme 2, related as they are to the half-life of the memory. An extremely slow rate of the conversion can be determined with a thin-layer cyclic voltammogram (TLCV).[8] An example of the TLCV is shown in Figure 2a obtained for complex **5** by a simulation. When the potential is increased, $1e^-$ oxidation takes place at 0.83 V, producing **A′**. Upon a

(15) Tomita, A. Ph.D. Dissertation, Nagoya University, 2000. The redox potential is 0.77 V (vs NHE) for *cis*-$[Ru(NH_3)_4(py)(pz)]^{2+}$ and 0.45 V for O-coordinated and 1.29 V for S-coordinated *cis*-$[Ru(NH_3)_4(dmso)(pz)]^{2+}$.

(16) The rates of the isomerizations above 40 s^{-1} are estimated by extrapolation from results at low temperatures.

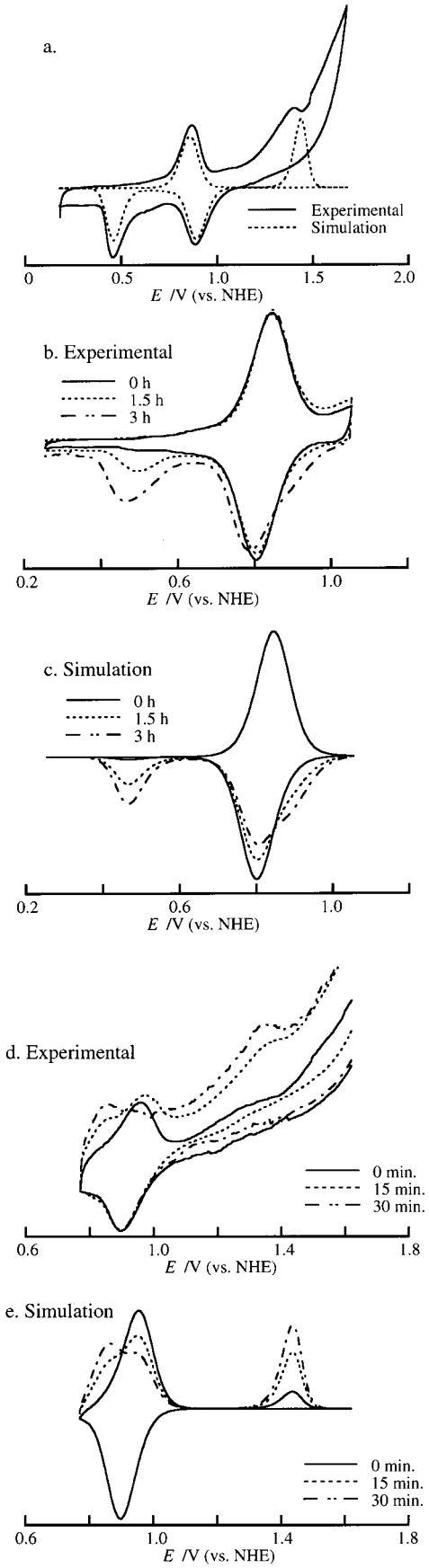

Figure 2. Thin layer cyclic voltammograms and digital simulations at 1 mV s^{-1} on acetone solutions containing *cis*-,*cis*-$[(NH_3)_4(py)Ru(pz)Ru(NH_3)_4(dmso)]^{4+/6+}$ (1 mM) and *n*-Bu_4NPF_6 (0.5 M) at 25 °C.

further increase in the potential to about 1.48 V, the fully oxidized species **A″** is formed, which isomerizes to **B**. Upon decrease of the applied potential, two reduction waves are obtained. The simulation (the dotted line in Figure 2a) of the above scheme without the conversion is in good agreement with the experiment.

The results of a different approach to determine a very slow rate of interconversion are shown in Figure 2b,d. When the potential is increased in Figure 3b, $1e^-$ oxidation takes place at 0.83 V. Upon further increase in the potential up to 1.06 V, the formation of **A′** is completed. Then the potential is kept at 1.06 V for specific intervals (0, 1.5, and 3 h). Now the applied potential is decreased and the species of **A′** is reduced to **A** at 0.83 V. However, during the specific intervals, some of **A′** is converted to **B′** with a rate $k+$, immediately oxidized to form the species **B**. As a result, the amplitudes of two reduction waves at 0.92 and 0.45 V are proportional to the amount of this conversion. In Figure 2d, the potential is applied at 1.6 V in the thin layer cell to form the fully oxidized species **B**. When the potential is decreased, $1e^-$ reduction takes place at about 0.9 V. Further decreasing the potential to 0.77 V formed **A′** completely, and the potential is kept at 0.77 V for specific intervals (0 min., 15 min., and 30 min.). During the specific intervals, some of **B′** is converted to **A′** with a rate $k-$, immediately reduced to form the species **A**. As a result, the amplitudes of two oxidation waves at 0.83 and 1.48 V are proportional to the amount of this conversion.

For the digital simulation of the results of TLCV, the reaction order for the conversion is needed. That it is first order is established by the observed independence of the amplitude of the reduction wave at 0.45 V on concentrations (0.37 and 3.7 mM). The TLCV data were simulated with variable parameters of rates $k+$ and $k-$ of forward and reverse reactions. Figure 3c,e shows the best fitting results with $k+ = 4.0 \times 10^{-5}$ s^{-1} and $k- = 3.8 \times 10^{-4}$ s^{-1}. Consequently the equilibrium constant $K = k+/k-$ between the mixed valence species is 0.11 for complex **5**. The above procedure was also successfully applied to determine the rates and the equilibrium constants of the conversions for the other complexes **4** and **6**.

Redox Potentials, Equilibria, and Dynamics for the Double-Block Reaction Scheme. The data on the redox potentials, the equilibrium constants, and the dynamics for the complexes studied here as based in Scheme 2 are summarized in Table 2. The redox potentials of E_1 and E_3 which apply to $[Ru^{2+/3+}\text{-}\text{-}Ru^{2+}SO]$ and $[Ru^{3+/2+}\text{-}\text{-}Ru^{2+}OS]$, respectively, show more positive shifts in the order **4** < **5** < **6**, while E_2 and E_4 show only small changes. In the mononuclear complexes, $[Ru(NH_3)_5(pz)]^{2+/3+}$, *cis*-$[Ru(NH_3)_4(py)(pz)]^{2+/3+}$, and *cis*-$[Ru(NH_3)_4(py)(pz)]^{2+/3+}$, redox potentials are obtained at 0.56, 0.77, and 0.93 V, respectively, close to the corresponding values for the E_1 and the E_3 in Table 2. That the values of E_3 are higher than those of E_1 is attributable to the greater electron-withdrawing effect of the counterpart couple when ruthenium is in the higher oxidation state.

The rates of the conversions, $k+$ and $k-$, increase and decrease, respectively, and the equilibrium constants, $k+/k-$, increase in the order of **4**, **5**, and **6**. The isomerization rates for **A″** → **B** and **B″** → **A** are almost unchanged, while equilibrium constants K_1 and K_2 decrease and increase, respectively, in the order of **4**, **5**, and **6**.

Discussion

The Lifetime of Memory. The production of either of the intermediate states **A′** or **B′** (see Scheme 2) constitutes storage of memory. Interconversion leads to loss of memory, and thus the rate of this interconversion is an important parameter of the

Table 1. Thermodynamics and Redox Potentials of the Isomerizations for dmso Complexes at 25 °C

		$[Ru^{2+}O] \rightarrow [Ru^{2+}S]$			$[Ru^{3+}S] \rightarrow [Ru^{3+}O]$	
compd	$E_{1/2}$ of $Ru^{2+/3+}O$/V	k/s^{-1}	$\Delta G°$/kJ mol^{-1}	$E_{1/2}$ of $Ru^{2+/3+}S$/V	k/s^{-1}	$\Delta G°$/kJ mol^{-1}
cis-$[Ru(NH_3)_5(dmso)]^{2+/3+}$	0.07	20 ± 2	−63	0.97	0.64 ± 0.02	−24
cis-$[Ru(NH_3)_4(py)(dmso)]^{2+/3+}$	0.31	1.0 ± 0.06		1.16	5.0 ± 0.2	
cis-$[Ru(NH_3)_4(pz)(dmso)]^{2+/3+}$ [a]	0.45	0.07 ± 0.02	−49	1.29	12 ± 2	−32
4	0.41	0.2 ± 0.05	−34	1.46	51 ± 5	−55
5	0.45	0.15 ± 0.03	−42	1.48	66 ± 13	−47
6	0.48	0.2 ± 0.1	−45	1.46	49 ± 14	−40

[a] Temperature at 20 °C.

Table 2. Equilibrium and Rate Parameters for the Double-Block Scheme for the Complexes in Acetone at 25 °C

	E/V				k/s^{-1}				k/s^{-1}		k/s^{-1}	
compd	E_1	E_2	E_3	E_4	k_1	k_{-1}	k_1/k_{-1}	k_2	k_{-2}	k_2/k_{-2}	$k+$	$k-$
4	0.65	1.46	0.78	0.41	51	$>1 \times 10^{-8}$	$<4 \times 10^{9}$	0.2	$<2 \times 10^{-7}$	$>1 \times 10^{6}$	$<5 \times 10^{-6}$	4×10^{-4}
5	0.83	1.48	0.92	0.45	66	3×10^{-7}	2×10^{8}	0.15	1×10^{-8}	2×10^{7}	4×10^{-5}	4×10^{-4}
6	0.98	1.46	1.08	0.48	49	5×10^{-5}	9×10^{6}	0.2	3×10^{-9}	7×10^{7}	2×10^{-4}	5×10^{-5}

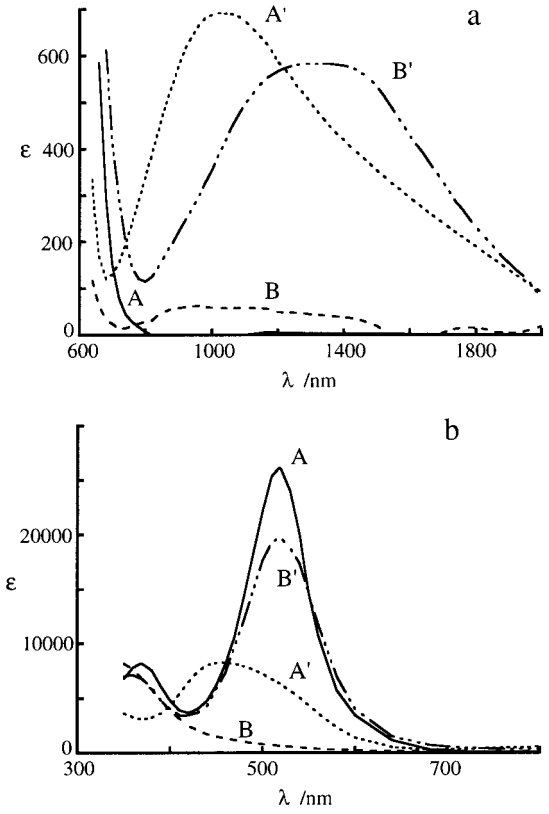

Figure 3. Absorption spectra of *cis*-,*cis*-$[(NH_3)_4(py)Ru(pz)Ru(NH_3)_4(dmso)]^{4+/5+/6+}$ (10.6 mM) and *n*-Bu_4NPF_6 (0.5 M) in acetone.

system. The approach to equilibrium is governed by ($k-$ + $k+$). We define the half-time for the approach to equilibrium, namely (ln 2)/($k-$ + $k+$), as the lifetime of the memory. These are 1.7×10^3, 1.6×10^3, and 2.8×10^3 s for species **4**−**6**, respectively. It must be emphasized that the lifetime of memory of molecule **6** is about 2.5 times longer than that (1100 s) of the molecule with the nonconducting bridging ligand previously reported,[8] even though a strong metal−metal interaction is introduced by pyrazine as a bridging ligand. It is indispensable to combine some electronic coupling and a longer lifetime of memory for applications of molecules of this kind in high-density memory storage, when light quanta are used to address the system. Our results lead to the conclusion that the stronger metal−metal interaction is compatible with a longer lifetime of memory in a molecule.

Isomerization Rates and Response in the System. In the application of molecular hysteresis to high-density memory storage, rapid response in the system is essential, and thus it is important to know what controls the rates of linkage isomerizations. Table 1 shows redox potentials, isomerization rates, and free energies for the dinuclear complexes together with data for some related mononuclear dmso complexes.[17] The finding is that rates of the isomerizations of $[Ru^{3+}SO] \rightarrow [Ru^{3+}OS]$ and $[Ru^{2+}OS] \rightarrow [Ru^{2+}SO]$ increase and decrease with increasing redox potentials for the complexes, respectively, in these systems. To realize rapid response in the system, the following molecular design is needed: in the isomerization of $[Ru^{2+}OS] \rightarrow [Ru^{2+}SO]$, the redox potentials of the complexes need to become more negative, and in the isomerization of $[Ru^{3+}SO] \rightarrow [Ru^{3+}OS]$, the rate can be increased by replacing methyl groups by bulky groups in the dmso,[16] leading to an acceleration of the isomerization in the system.

Equilibrium Constants between the Mixed-Valence Species and Redox Potentials. We now turn to a discussion of the increase of the equilibrium constants [**B′**]/[**A′**] in the order of **4**, **5**, and **6** with increasing values E_1 and E_3. The following equations apply to the dynamics of the system presented in Scheme 2:

$$+) \; [Ru^{3+}\text{--}Ru^{2+}SO] + e = [Ru^{2+}\text{--}Ru^{2+}SO] \quad E_1$$
$$-) \; [Ru^{2+}\text{--}Ru^{3+}OS] + e = [Ru^{2+}\text{--}Ru^{2+}OS] \quad E_4$$
$$-) \; [Ru^{2+}\text{--}Ru^{2+}OS] = [Ru^{2+}\text{--}Ru^{2+}SO] \quad RT/F \ln K_2$$
$$[Ru^{3+}\text{--}Ru^{2+}SO] = [Ru^{2+}\text{--}Ru^{3+}OS] \quad E_1\text{-}E_4\text{-}RT/F \ln K_2$$
$$) \; [Ru^{3+}\text{--}Ru^{3+}SO] + e = [Ru^{3+}\text{--}Ru^{2+}SO] \quad E_2$$
$$+) \; [Ru^{3+}\text{--}Ru^{3+}OS] + e = [Ru^{2+}\text{--}Ru^{3+}OS] \quad E_3$$
$$-) \; [Ru^{3+}\text{--}Ru^{3+}OS] = [Ru^{3+}\text{--}Ru^{3+}SO] \quad RT/F \ln K_1$$
$$[Ru^{3+}\text{--}Ru^{2+}SO] = [Ru^{2+}\text{--}Ru^{3+}OS] \quad -E_2+E_3-RT/F \ln K_1$$

Two equations $-F(E_1 - E_4 - (RT/F) \ln K_2)$ and $-F(-E_2 + E_3 - (RT/F) \ln K_1)$ are obtained as the free energies of the equilibria [**B′**]/[**A′**], where the equilibrium constant depends on the redox potentials E and the isomerization equilibrium constants K. The redox potentials of E_1 and E_3 increase from 0.65 to 0.98 V and from 0.78 to 1.08 V in the order of **4**, **5**, and **6**, respectively, while the values of E_2 and the E_4 are much less sensitive to the changes in composition. This is expected because only the reversible couple is affected directly by the

(17) Tomita, A.; Sano, M. *Inorg. Chem.* **1994**, *33*, 5825−5830.

Table 3. Absorption Spectra for the Complexes with Each Oxidation State.

	species/nm					
compd	**A** [Ru^{2+}- -Ru^{2+}SO]	**A′** [Ru^{3+}- -Ru^{2+}SO]		**B′** [Ru^{2+}- -Ru^{3+}OS]		**B** [Ru^{3+}- -Ru^{3+}OS]
4	520 (25 000)	445 (8700)	880 (920)	520 (19 000)	1570 (1700)	340 (8600)
5	517 (26 000)	455 (8400)	1010 (770)	518 (20 000)	1300 (640)	
6	498 (23 000)	450 (7500)	1120 (1100)	500 (17 000)	1060 (520)	

[a] Values in parentheses are the molar absorption coefficients.

changes in composition. The values of (RT/F) ln K_1 and (RT/F) ln K_2 are 0.57, 0.50, and 0.41 V and 0.31, 0.43, and 0.47 V for the complexes **4**, **5**, and **6**, respectively. Consequently in the equations the variations of E_1 and E_3 are dominant between the complexes. More positive values E_1 and E_3 give more negative values of $-F(E_1 - E_4 - (RT/F)\ \ln K_2)$ and $-F(-E_2 + E_3 - (RT/F)\ \ln K_1)$, leading to increasing equilibrium constants between the mixed-valence species.

Reading Out the Memory by Absorption of Light. In Figure 3 are shown the absorption spectra covering the near-infrared and visible regions for each accessible state based on complex **4**. They are obtained in acetone by use of thin-layer electrochemical cells.[18] Only the mixed-valence states **A′** and **B′** show strong absorption in the near-infrared region—the small absorption shown by **B** in this energy region is probably caused by an impurity.

The absorptions of **A′** ($\lambda_{max} = 1010$ nm) and **B′** ($\lambda_{max} = 1300$ nm) (Table 3) are intervalence transitions assignable to [Ru^{2+}-SO] → [Ru^{3+}] and [Ru^{2+}] → [Ru^{3+}OS], respectively. Their high intensity relative to those of the isovalent forms and the difference in λ_{max} for **A′** and **B′** qualify them as a means of reading out the memory.

The energies of the intervalence (IT) bands for **A′** and **B′** decrease and increase respectively in the order, **4**, **5**, and **6**. These trends are in line with the redox potentials of the relevant couples as summarized in Table 2. It has already been noted that while the changes in potential for the DMSO couples in the series are small—ΔE in the most extreme case is 0.07 V—those for the reversible couple are greater than 0.30 V. This difference in sensitivity is expected because, within the series, the immediate environment only of the metal atom in the reversible couple is changed. This couple becomes more strongly oxidizing in the order **4**, **5**, and **6**, which decreases the energy of the [Ru^{2+}-SO] → [Ru^{3+}] transition (**A′**), the order being reversed for [Ru^{2+}] → [Ru^{3+}OS] (**B′**).

In reference to the visible region of the spectrum, we note in Figure 3b an intense ($\epsilon = 24\,700\ M^{-1}\ cm^{-1}$) absorption for **A** [$Ru^{2+}$- -$Ru^{2+}$SO] and **B** [$Ru^{3+}$- -$Ru^{3+}$OS] but no corresponding bands for **A′** [Ru^{3+}- -Ru^{2+}SO] and **B** [Ru^{3+}- -Ru^{3+}OS]. Thus the absorption can be assigned to $Ru^{2+} \rightarrow \pi^*$(pyrazine). Absorption for **A′** in the complex **4** is observed at 450 nm, which is almost the same as those in the other complexes **5** and **6** where it is assigned to [OSRu^{2+}] → π^*(pyrazine).

Acknowledgment. We are grateful to Prof. H. Taube of Stanford University for his encouragement and for his critically reviewing the manuscript. We thank Presto21 of the JRDC, Sumitomo Foundation, and the Tatematsu Foundation for supporting the present work.

IC9814219

(18) Each oxidation state (**A′**, **B′**, and **B**) was prepared by electrolysis of **A** in the thin-layer electrochemical cell. The spectra were successively measured in a series of **A**, **A′**, **B**, **B′**, and **A** in a same solution. The extent of decomposition in the solutions during the experiments was checked by comparing the first and the last measurements for **A**.